Barbara Canonico, Luca Giorgi, Maria Gemma Nasoni, Mariele Montanari, Gianluca Ambrosi, Mauro Formica, Caterina Ciacci, Patrizia Ambrogini, Stefano Papa, Vieri Fusi and Francesca Luchetti*

Synthesis and biological characterization of a new fluorescent probe for vesicular trafficking based on polyazamacrocycle derivative

https://doi.org/10.1515/hsz-2021-0204
Received April 1, 2021; accepted May 25, 2021;
published online June 7, 2021

Abstract: The fluorescent probes represent an important tool in the biological study, in fact characterization of cellular structures and organelles are an important tool-target for understanding the mechanisms regulating most biological processes. Recently, a series of polyamino-macrocycles based on 1,4,7,10-tetraazacyclododecane was synthesized, bearing one or two NBD units (AJ2NBD·4HCl) useful as sensors for metal cations and halides able to target and to detect apolar environment, as lipid membranes. In this paper, we firstly illustrate the chemical synthesis of the AJ2NBD probe, its electronic absorption spectra and its behavior regarding pH of the environment. Lack of any cellular toxicity and an efficient labelling on fresh, living cells was demonstrated, allowing the use of AJ2NBD in biological studies. In particular, this green fluorescent probe may represent a potential dye for the compartments involved in the endosomal/autophagic pathway. This research's field should benefit from the use of AJ2NBD as a vesicular tracer, however, to ensure the precise nature of vesicles/vacuoles traced by this new probe, other more specific tests are needed.

Keywords: autophagy; endo-lysosomes; NBD; poly-azamacrocycle; rapamycin; starvation.

Barbara Canonico and **Luca Giorgi** contributed equally to this work.

***Corresponding author: Francesca Luchetti**, Department of Biomolecular Sciences, University of Urbino Carlo Bo, I-61029 Urbino, Italy, E-mail: francesca.luchetti@uniurb.it

Barbara Canonico, Maria Gemma Nasoni, Mariele Montanari, Caterina Ciacci, Patrizia Ambrogini and Stefano Papa, Department of Biomolecular Sciences, University of Urbino Carlo Bo, I-61029 Urbino, Italy

Luca Giorgi, Gianluca Ambrosi, Mauro Formica and Vieri Fusi, Department of Pure and Applied Sciences, University of Urbino Carlo Bo, I-61029 Urbino, Italy

Introduction

Study and characterization of cellular structures and organelles are an important tool-target for understanding the mechanisms regulating most biological processes. In this field, the best technique used is confocal fluorescence microscopy due to its high sensitivity and resolution, thus researchers are ongoing needing new and efficient fluorescent probes with improved selectivity for specific cell organelles (Wang et al. 2019; Xu et al. 2016; Zhu et al. 2016). The cellular organelles are surrounded by lipid membranes having a specific composition and peculiar characteristics of permeability, lipid packing and elasticity. Different fluorescent probes containing a wide variety of fluorophores suitable to visualize the lipid membranes are reported in the literature (Dick et al. 2014). Recently a series of NBD-based polyamine macrocyclic fluorescent probes, some of them able to modulate their optical emission properties in the presence of selected metal cations, halide anions and by solvent polarity, has been synthesized by our research group (Amatori et al. 2012, 2014; Ambrosi et al. 2009; Arca et al. 2014). Being fluorescent probes important tools in the biological study we have focused our attention on this topology with the aim to investigate in depth the fluorescent behavior in the living cell of one of them as a possible probe for lipid membranes. The attention has been focused on one of them here called AJ2NBD (Papa et al. 2019); it is a NBD-based probe which synthetic obtainment has here been improved as well as its photochemical behavior in solution studied in depth.

The endo-lysosomal compartments and autophagosomes represent an important apparatus able to maintain the homeostasis within the cells. This apparatus consists of endosomes, retromers, autophagosomes and lysosomes. The endosome is the major sorting compartment that transports proteins and other cargos to and from Golgi apparatus. In parallel, protein and lipid from the plasma membrane are transported through the generation of early endosomes. The cargo can be recycled to the plasma membrane or retained in

the late endosomes which finally can fuse with lysosomes for the degradation of the cargo (Cao et al. 2019; Schreij et al. 2016).

Autophagy is involved in cell function and survival. During autophagy, the cytoplasmic components such as misfolded proteins and damaged organelles are engulfed by an isolation membrane that elongates to form an autophagosome. The autophagosomes fuse with endosomes and lysosomes to acquire proteases and lipases (Ravikumar et al. 2010). To this regard, Razi and coworkers provided direct evidence that fusion of autophagic vacuole with early endosomes represent a key step in the autophagic process (Razi et al. 2009). Successful autophagy occurs as a response to initial stress that may be a pathogen, damaged organelles and starvation.

In this paper we firstly illustrate the chemical synthesis of the AJ2NBD probe, its electronic absorption spectra and its behavior regarding pH of the environment. Then, we show the feasibility of AJ2NBD use in biological studies, pointing out the lack of any cellular toxicity and an efficient labelling on fresh cells but not on paraformaldehyde-fixed cells. Finally, coupling confocal and flow cytometric studies, we demonstrated that this green fluorescent probe can be adopted as a potential dye for the compartments involved in the endosomal/autophagic pathway. This research's field should benefit from the use of AJ2NBD as a vesicular tracer.

Results

Synthesis of AJ2NBD

The probe AJ2NBD (1,7-bis-(7-nitrobenzo[1,2,5]oxadiazole-4-yl)-4,10-dimethyl-1,4,7,10- tetraazacyclododecane was firstly obtained by coupling 1,7-dimethylcyclen (1) (Ciampolini et al. 1984) with NBD-Cl (4-chloro-7-nitrobenzo[1,2,5] oxadiazole) (2) in toluene together with the monosubstituted analog 1-(7-nitrobenzo-1,2,5]oxadiazole-4-yl)-4,10-dimethyl-1,4,7,10-tetraazacyclododecane (Ambrosi et al. 2009). The synthesis has been improved using two equivalents of NBD-Cl (2) and performing the reaction in acetonitrile in the presence of an alkaline carbonate base at room temperature, following the pathway depicted in Scheme 1. Under these conditions the probe can be easily obtained and purified as tetrahydrochloride salt with an overall yield of 80%.

Photochemical properties in aqueous solution

The probe AJ2NBD contains two aliphatic and two aromatic amine functions thus possess acid-base properties and can be present in aqueous solution as different protonation forms depending on the pH. Tetrahydrochloride salt of AJ2NBD precipitates from highly concentrated hydrochloric acidic ethanolic solution (see synthesis chapter) suggesting that, in principle, all the four amine function can be protonated giving rise to $H_4AJ2NBD^{4+}$ species. This species surely exists in a strongly acidic solution, but in the pH range 2–11, in which pH is easily and precisely measurable, less protonated forms can be stable. The net charge of the species that prevails in solution can strongly affect the photochemical properties and the distribution of the probe in the cellular comparts, then with the aim to understand which species are effectively present in aqueous solution as a function of the pH a series of spectrophotometric and spectrofluorimetric acid-base titrations has been performed in the 2–11 pH range maintaining the ionic strength constant (I = 0.15 M NaCl).

At pH = 2 the absorption spectrum of the probe shows the two typical bands of 4-amino-7-nitro disubstituted benzofurazan moieties at 340 nm (ε = 12,500 cm^{-1} mol^{-1} dm^3) associated with π–$\pi^\star$ transition and at 457 nm (ε = 27,500 cm^{-1} mol^{-1} dm^3) attributed to intramolecular charge transfer (CT) from the aromatic amines to NBD ring (Figure 1A) (Uchiyama et al. 1998, 1999). Increasing the pH both bands were red-shifted displacing towards 355 and 475 nm at pH = 11. Moreover, at pH up to 10 a third

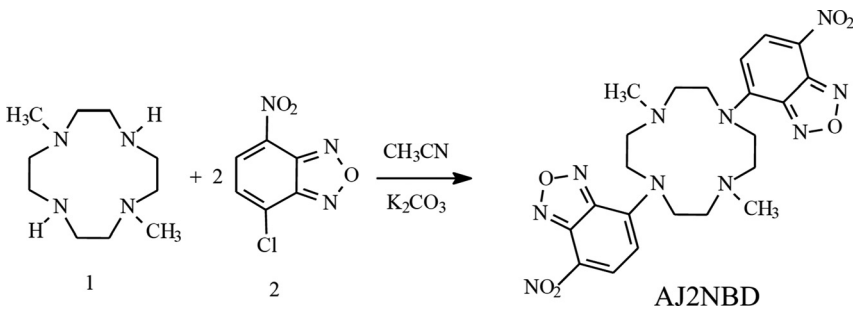

Scheme 1: Synthetic pathway of AJ2NBD probe.

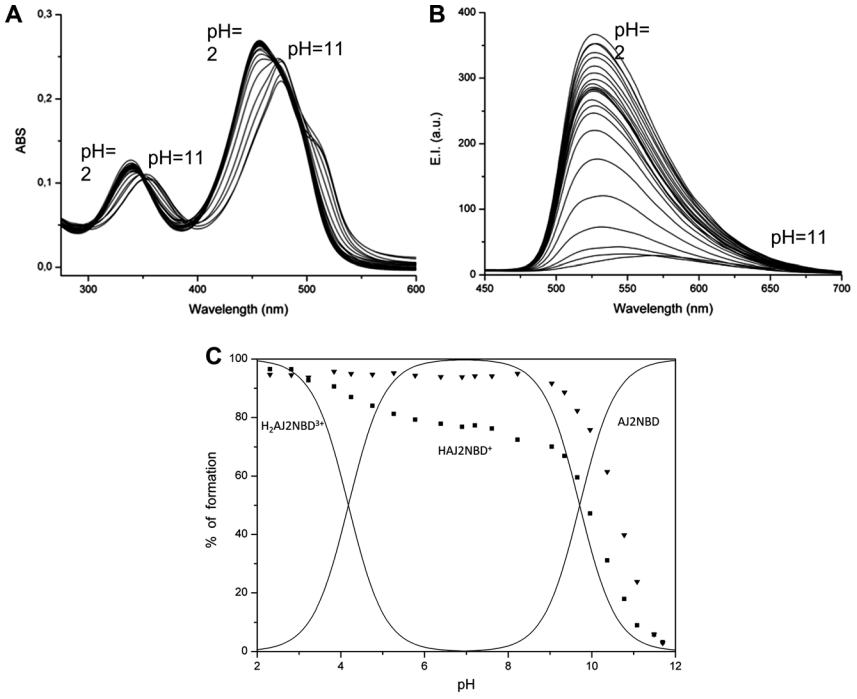

Figure 1: Spectroscopic behavior in aqueous solution.
(A) Electronic absorption spectra. (B) Emission spectra of AJ2NBD (λ_{ex} = 350 nm) in aqueous 0.15 M NaCl at various pH values. (C) Distribution diagram of AJ2NBD species in aqueous solution as a function of pH at 298 K with relative trend of absorbance at 457 nm (▼) and fluorescence emission intensity at 527 nm (■) ([AJ2NBD] = 10^{-5} mol dm^{-3}, 298 K, I = 0.15 mol dm^{-3} NaCl).

absorption band, observable as a shoulder at 510 nm, appears.

pH-dependent fluorescence emission spectra were recorded upon exciting at the isosbestic point (λ_{ex} = 350 nm) near to π–π* transition because this absorption band is less influenced by pH respect to the CT one. In acidic solution, the ligand is fluorescent with an emission quantum yield of φ_{fl} = 0.05 and the maximum emission at λ_{em} = 527 nm (Figure 1B), successively the emission intensity decreases along with the increase of pH. Starting from pH = 2 and going to higher pH values a drop in emission intensity occurs at pH about 4.5 reaching a reduction of 15% of the initial intensity up to pH = 6.0, then a second and more significant drop in emission intensity starts at pH = 9, bringing to the loss of more than the 95% of emission intensity up to pH = 11.5. Merging the absorption and the emission spectra collections and analyzing the changes that occur as a function of pH we can suppose that in the pH range 2–11 the two protonation forms $H_2AJ2NBD^{2+}$, $HAJ2NBD^{+}$ and the neutral AJ2NBD species exist.

This hypothesis is supported by the speciation described in the literature by the 1,7-dimethylcyclen macrocycle system (Ciampolini et al. 1984). By processing the fluorescence pH-metric titration using the HypSpec program (Gans et al. 1996), the two deprotonation constants of $\log K_1$ = 9.71 and $\log K_2$ = 4.17 were estimated (Table 1). Figure 1C reports the distribution diagram of the species as a function of pH superimposed with the trends of the absorption at 427 nm emission intensity at 527 nm. Following this data and looking at the absorption spectra, starting from pH = 2, when the deprotonated $H_2AJ2NBD^{2+}$ prevails in solution, the red-shift observed in the absorption bands along the increase of pH is attributable to the deprotonation steps of the macrocycle nitrogen atoms that, increasing the availability of the aromatic amine lone pairs, extend the conjugate system of both NBD groups displacing the absorption bands toward lower energy.

More information can be obtained from the trend of the fluorescence emission intensity at 527 nm as a function of pH. The emission intensity undergoes a general loss in emission intensity along with the increase of pH suggesting that the probe is a PET-regulated probe in which the excited state of the fluorophore is quenched by the photoinduced electron transfer from the lone pair of the aliphatic amine function to the NBD systems (Formica et al. 2012). At pH = 2, when the deprotonated $H_2AJ2NBD^{2+}$ specie prevails, the emission reaches its maximum intensity because the two

Table 1: Protonation constants of AJ2NBD spectrofluorimetrically determined at 298 K (I = 0.15 M NaCl).

Reaction	Log *K*
$AJ2NBD + H^+ = HAJ2NBD^+$	9.71(1)[a]
$HAJ2NBD^+ + H+ = H_2AJ2NBD^{2+}$	4.17(1)

aliphatic amine groups of the macrocycle are protonated this PET is forbidden. The drop in emission intensity that occurs at pH about 4.5 (15% reduction) can be ascribed to the first deprotonation step in which the $HAJ2NBD^+$ specie appears in solution; in this monoprotoned species, the proton is shared between the two aliphatic amines partially allowing PET. The second and more significant drop in emission intensity, starting at pH = 9.5 and leading to the loss of more than the 95% of emission intensity up to pH = 11.5. It reflects the last deprotonation step giving rise to the neutral species in which both aliphatic amines are deprotonated, thus the overall fluorescence is quenched by the PET effect (Supplementary Figure 1).

Solvatochromic effect

Further photochemical characterizations of AJ2NBD were carried out acquiring the UV–Vis absorption and emission spectra in different solvents. For this purpose, the ligand purified as tetrahydrochloride salt has been previously extracted from an alkaline sodium hydroxide solution with chloroform, dried and evaporated to obtain AJ2NBD as free amine with a yield of 60%. It is well known that spectral positions, absorption coefficients and emission quantum yield of a molecule may be strongly influenced by the environment. In fact, solvation influences the stability of electronic ground and excited states as well as the orientation of substituent groups affecting in turn their participation in the electronic structure of the conjugate systems. Moreover, the fluorescence emission quantum yield is the result of the competition of radiative and non-radiative transitions, the last comprising, photoinduced electron transfer (PET) that usually quenches the system and photoinduced charge transfer that displaces the emission band. Knowing the photochemical behavior of a molecule in different environments allows us to understand the nature of excited state. Table 2 reports the absorption (CT) and emission bands wavelengths, the stokes shifts (Δ_{ss}) and the fluorescence quantum yields (φ_{fl}) of the probe in selected solvents having different relative dielectric constants (ε_r) and different capability to donate H-bond, this last expressed as the Feller fh parameter. The solvent in which the ligand is more fluorescent is methanol, followed by ethanol, acetone, dioxane and water. Due to its basicity, in aqueous solution the probe is present as monoprotonated form $HAJ2NBD^+$, as confirmed by the quantum yield. The absorption wavelength decreases together with the H-bond donor capability of solvent confirming that the emissive low excited state is CT, namely the unbonded lone pair of the aromatic amine linked to NBD plays a crucial role in the absorption and emission properties. Stokes shift increases along with the capability of solvent to donate H-bond due to the stabilization of fundamental state and destabilization of the excited one. Fluorescence quantum yield is strongly influenced by the dielectric constants and H-bond donor capability of the solvent, as reported in Supplementary Figure 2, showing a maximum for methanol. This behavior can be rationalized taking into account that when the main mechanism that influences the emission quantum yield is PET, as in this case, the dielectric constant and the H-bond donor tendency of the solvent show opposite effects. The electron transfer from the aliphatic amine lone-pairs to the excited fluorophore have a spatial character, in other words an electron that leaves the nitrogen atom travels through the space in order to reach the fluorophore overcoming the local electric field generated by the ionized donor atom. A higher dielectric constant of the solvent correlates with a lower local electric field intensity allowing the PET process. Otherwise the ability of the solvent to donate H-bond stabilizes the nitrogen lone pairs lowering its oxidation potential thus hampering PET. In this context, most probably methanol presents the better compromise between dielectric constant and H-bond capability for AJ2NBD making it more fluorescent than in other solvents. In general, the emission of the probe is more intense in organic media than in aqueous solution.

Table 2: Spectrophotometric parameters of **L** in different solvents.

Solvent	ε_r	fh	λ_{abs} (nm)	λ_{em} (nm)	Δ_{ss} (cm^{-1})	φ_{fl}
Water	80.1	58	455	527	3003	0.043
Methanol	33.6	48	470	525	2229	0.370
Ethanol	24.3	45	478	531	2088	0.230
Acetone	20.7	21	480	521	1639	0.140
Dioxane	2.20	–	480	524	1749	0.210

AJ2NBD staining

In order to evaluate the potential cytotoxicity of AJ2NBD, we evaluated the percentage of viable cells after AJ2NBD staining, compared with other commercial probes (MTR, LTDR and Bodipy). Our results show that the percentage of viable cells is close to that one of control samples and very similar for all probes investigated suggesting that AJ2NBD is suitable for biological studies (Figure 2A). Moreover, our results show that AJ2NBD exhibits a dose-dependent uptake in the FL1 channel (emission wavelengths), hence the choice to apply this channel for the following investigations (Figure 2B). Interestingly, the

labeling after 24 h of incubation at +4° showed a similar pattern exhibiting a dose-dependent uptake in the FL1 channel in both cell lines (Supplementary Figure 3). This confirms the stability of the fluorescent signal and the specific labelling for up to 24 h.

AJ2NBD is able to diffuse across the plasma membrane. In particular, the fluorescent substance is capable of staining the perinuclear region in both cell lines, as depicted in Figure 2C. It is possible to observe a weak diffuse fluorescence in the cytoplasm, whereas a specific and bright fluorescence labels the region close to the nuclear membrane in a punctate feature distribution.

To verify whether AJ2NBD was suitable to stain fixed cells, we compared the AJ2NBD labelling in live HT22 and in 4% paraformaldehyde (15 min RT) HT22 fixed cells. The results shown in the Supplementary Figure 4 indicate that the fluorescent probe AJ2NBD is not correctly suitable in fixed cells. The cytometric analyses show a significant increase (**$p < 0.01$, ***$p < 0.001$) of mean fluorescence intensity (MFI) of AJ2NBD in viable and fixed HT22 cells if compared to the unlabeled condition. However, the results show an increase of MFI in unstained HT22 fixed cells besides a decrease of MFI in AJ2NBD labelled cells ($p < 0.01$) if compared to viable HT22 cells. Furthermore, the confocal

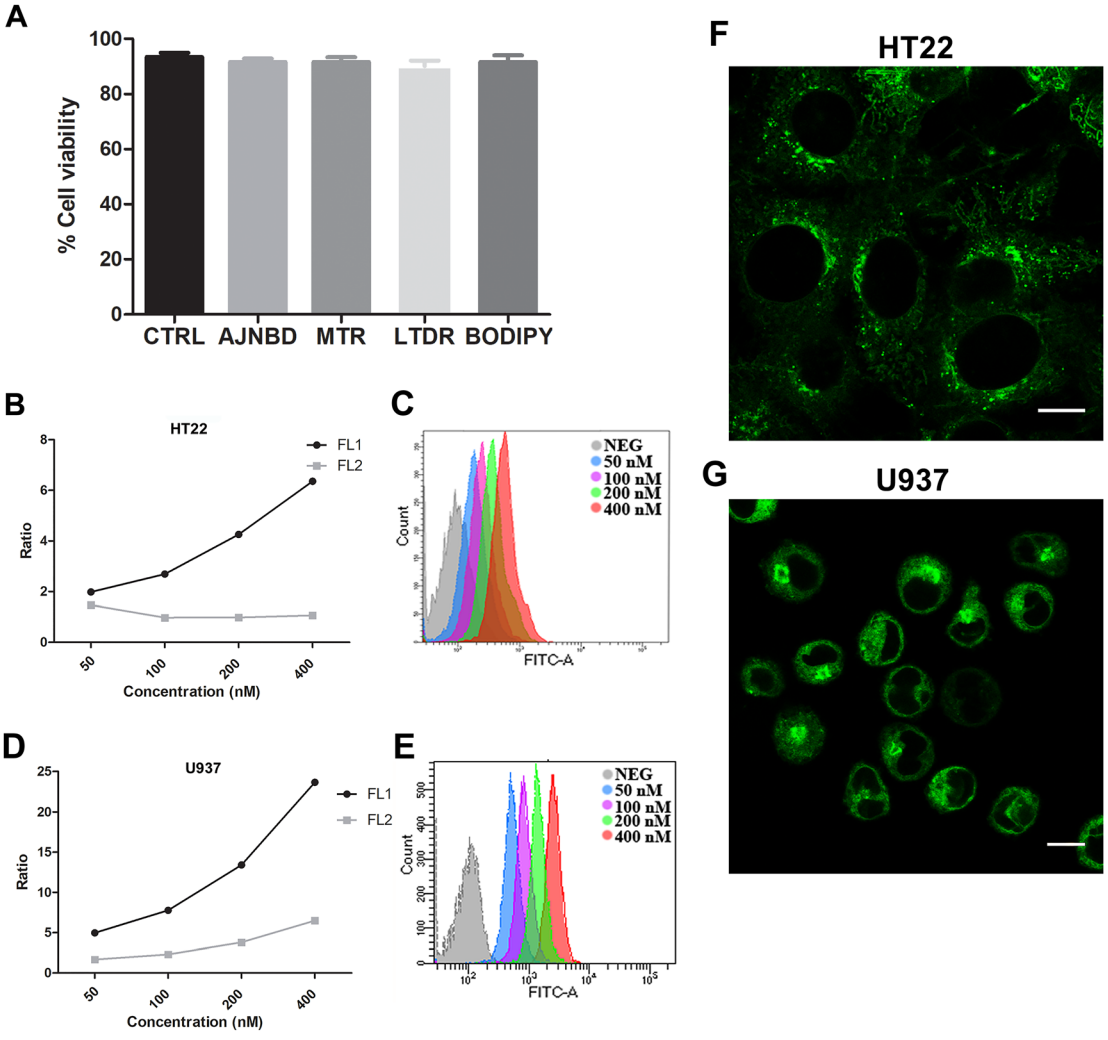

Figure 2: Staining of AJ2NBD probe in U937 and HT22 cell lines.
(A) Statistical histogram of the percentage of viable cells after the staining with AJ2NBD, MitoTracker Red (MTR), LysoTracker Deep Red (LTDR) and Bodipy compared to ctrl. (B) Trends of AJ2NBD ratio for HT22 at different concentrations (50, 100, 200 and 400 nM). (C) Cytometry histogram of AJ2NBD MFI at different concentrations. (D) Trends of AJ2NBD ratio for U937 cell lines at different concentrations (50, 100, 200 and 400 nM). (E) Cytometry histogram of AJ2NBD MFI at different concentrations. (F, G) Single confocal optical sections of HT22 and U937 cells stained by AJ2NBD. Scale bar: 10 µm. Each value is expressed as the mean ± SD (results from $n \geq 3$ independent experiments).

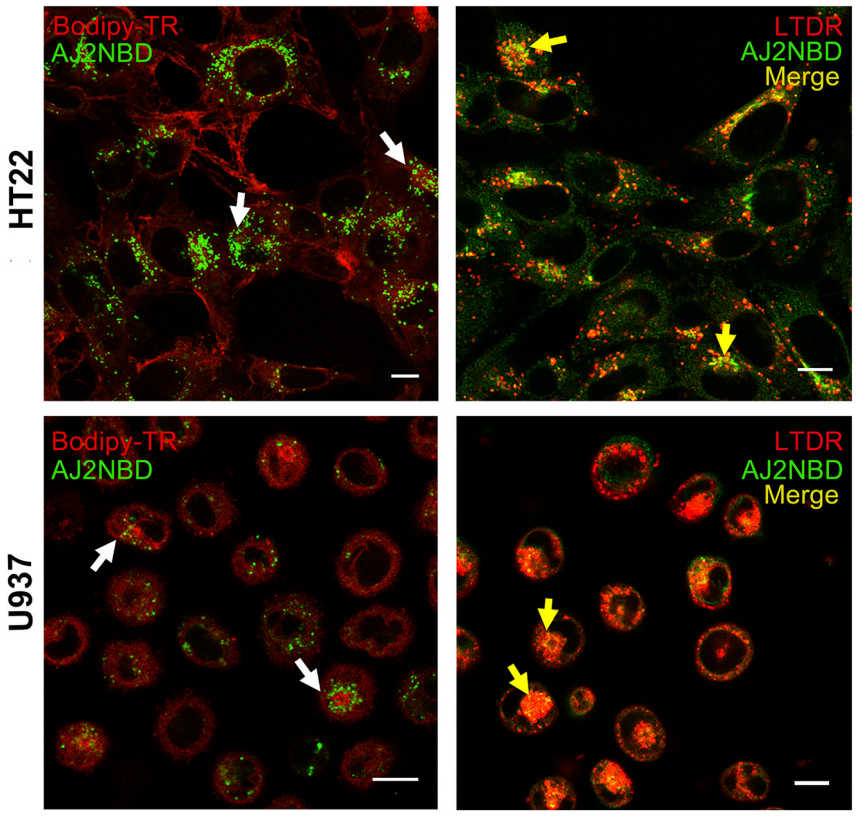

Figure 3: Confocal images obtained by colocalization between AJ2NBD and bodipyTR ceramide and LTDR.
The white arrows indicate the AJ2NBD staining around the peripheral region of Golgi in both cell lines. On the contrary, the yellow arrows highlighted the colocalization between AJ2NBD and LTDR in the same peripheral region of Golgi. Scale bar: 10 µm.

analyses demonstrate an extremely widespread labeling not attributable to any organelle, attesting a significant fluorescence diffusion and confirming that AJ2NBD is not suitable for biological studies on fixed cells.

AJ2NBD specifically stains the vesicles around the Golgi

The biological studies are characterized by the simultaneous application of different probes in live cells in order to identify specific organelle and structures. Strictly regarding confocal analyses, we firstly take into account photostability. In fact, in all control samples, fluorescence intensity remains stable and homogeneous during the whole time of the analyses suggesting that the probe is resistant to photobleaching.

Two different cell lines were co-labeled with AJ2NBD and several commercial probes. Results (Supplementary Figure 5) show that the ex/em of AJ2NBD is consistent with the ex/em of several commercial probes. The colocalization has been evaluated by Pearson coefficient and the obtained values show, in U937 cells, only a negligible colocalization with MTR (p = 0.568) and a greater colocalization with LTDR (p = 0.707). On the contrary, the Pearson coefficient obtained for HT22 with the same probes show a significant decrease in the colocalization suggesting a basal expansion of this AJ2NBD+ compartment for the adherent, neuronal cells and, contemporary, an easier and more specific visualization. In detail, both cell lines investigated showed a greater co-localization with the LDTR (p = 0.574) if compared to MTR (p = 0.376).

The specific colocalization with lysosomes lead us to investigate a possible link with AJ2NBD and BodipyTR ceramide, a specific probe for Golgi apparatus. Our results demonstrate that AJ2NBD specifically stains the region around the Golgi (Figure 3, white arrow), although not colocalizing with BodipyTR: in fact, we observed the appearance of numerous small vesicles in the Juxta-Golgi region in both cell lines investigated (Figure 3), exhibiting green fluorescence not overlapping with red one. On the other hand, the labelling with LTDR confirms its partial colocalization with AJ2NBD probe, identified by yellow punctate around Golgi apparatus (Figure 3, yellow arrow).

AJ2NBD and AO labelling of starved and rapamycin-treated cells

A major response to nutrient starvation is the stimulation of the degradative pathway identified as macroautophagy and also referred as autophagy, a process inducible by both

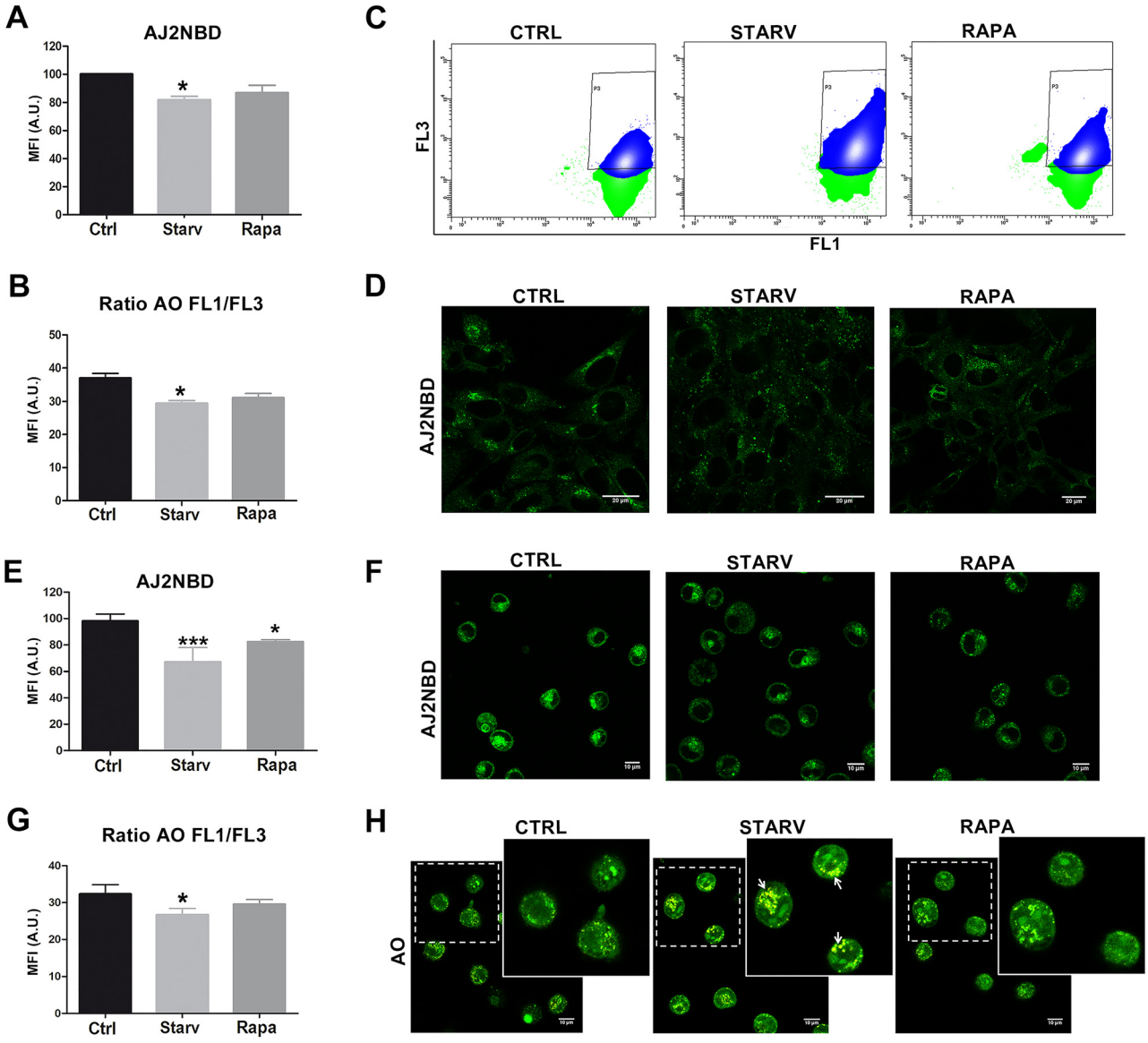

Figure 4: Evaluation of acidic vacuoles by AJ2NBD and AO labelling in U937 and HT22 cell lines.
(A) Statistical histogram of AJ2NBD MFI on HT22 cells ctrl, starved and rapamycin-treated cells. (B) Statistical histogram of ratio FL3/FL1 of acridine orange (AO) on HT22 ctrl, starved and rapamycin-treated cells. (C) Contour plot of FL1 and FL3 of AO for ctrl, starved cells and HT22 treated with Rapamycin. (D) Single confocal optical sections of HT22 ctrl, starved and rapamycin-treated cells stained by AJ2NBD. Scale bar: 20 µm. Each value is expressed as the mean ± SD (results from $n \geq 3$ independent experiments); one-way ANOVA with Bonferroni's multiple comparison test revealed: $*p < 0.05$, vs. control. € Statistical histogram of AJ2NBD MFI on U937 cells ctrl, starved cells and cells treated with rapamycin. (F) Single confocal optical sections of U937 cells (ctrl), starved (Starv) and treated with Rapamycin (Rapa) staining by AJ2NBD. Scale bar: 10 µm.
(G) statistical histogram of ratio FL1/FL3 of acridine orange (AO) on U937 ctrl, starved and Rapamycin treated cells. (H) Confocal images of U937 cells (ctrl), starved (Starv) and treated with Rapamycin (Rapa) staining by AO. The enlarged inserts show the overlay of FL1 and FL3. The white arrows highlighted the numerous yellow punctate in the Starv condition. Scale bar: 10 µm. Each value is expressed as the mean ± SD (results from $n \geq 3$ independent experiments); one-way ANOVA with Bonferroni's multiple comparison test revealed: $*p < 0.05$, and $***p < 0.001$ vs. control.

serum starvation (Starv) and rapamycin administration (Rapa) (Klionsky et al. 2021). To deeply investigate the effects of the two autophagy inducers (Starv and Rapa), we labelled cells by MDC probe, quantifying fluorescence intensity by flow cytometry. Flow cytometric data (see Supplementary Figure 6) show a strong increase of autophagy-related vesicles in HT22 starved and rapamycin-treated cells ($***p < 0.001$), whereas in U937 cells this increase is significant only in rapamycin treated cells ($*p < 0.05$). Endosomes and autophagosomes sequester their distinct cargos via different mechanisms, yet they converge at the level of lysosomes as their common degradative endpoint.

To evaluate the possibility to apply AJ2NBD in studying processes in which vesicular formation and trafficking play a key role, we labelled control, starved and rapamycin-treated U937 and HT22 cells. Firstly, we provide an AJ2NBD fluorescence quantitation by flow cytometry in HT22 adherent cells and we compare this trend with those from acridine orange (AO) labelling. In fact, this metachromatic probe is able to evaluate both more acidic (FL3) and less acidic (FL1) vacuoles, that usually are referred as early endosomes, since they are still not mature and are acidified to pH 6.2 by V-ATPase (Canonico et al. 2018; Marshansky and Futai 2008). The ratio FL1/FL3 takes into account these probe's capabilities. AJ2NBD trends for control, starved and rapamycin-treated HT22 cells are the same highlighted by AO labelling (Figure 4A and B).

In particular, our results show a significant decrease of AJ2NBD MFI and AO ratio of FL1/FL3 MFI ($p^\star < 0.05$) in HT22-starved cells, suggesting a greater induction of the acid-lysosomal compartment. The concomitant cytometric analysis of AO labelling and confocal microscopy of AJ2NBD staining confirm these data. The contour plot of AO (Figure 4C) shows a higher FL3 positive population (blue region, P3) and a decrease of FL1 positive cells in HT22-starved cells compared to Ctrl and rapamycin conditions. Confocal HT22 images of AJ2NBD staining pointing out a less punctate green fluorescence diffused in the cytoplasm in HT22-starved cells, while a bright punctate green fluorescence around the nucleus in Ctrl and rapamycin-treated samples (Figure 4D). Contemporary U937 floating cells exhibit the same behavior, but AJ2NBD demonstrates a more significant tracing of the two treatments ($^\star p < 0.05$, and $^{\star\star\star}p < 0.001$) (Figure 4E). The confocal images obtained by AJ2NBD staining underline the brilliant punctate-vesicular fluorescence in Ctrl condition and a weaker and diffuse green fluorescence in Starv and rapamycin-treated cells (Figure 4F). The AO staining confirms the trend obtained by AJ2NBD labelling (Figure 4G). In particular, in U937-starved cells the decrease of the ratio FL1 and FL3 of AO (flow cytometric quantitation) may be transposed in the bright yellow punctate fluorescence (confocal analyses) that confirm the increase in more acid vacuoles (Figure 4H).

AJ2NBD labelling pattern highlights correlation and complementarity with LTDR

Lysosome quantification by LTDR staining highlights that, applying the two different triggers, is possible to follow intracellular acidic vacuole and vesicle movements (Figure 5A). Furthermore, confocal images are in absolute agreement with flow cytometric investigations, as depicted in Figure 5B. This further analysis on LTDR fluorescence allows an in depth comparison of acidic compartment between starvation and rapamycin treatments. As observable, these two triggers involve the lysosome network to a different extent (Figure 5A). This could, together with autophagy-related vacuoles, corroborate the trend of AJ2NBD probe, showing a different distribution and quantitative fluorescence between starved and rapamycin-treated cells (Figure 5B). Several researchers start to point out these differences, in fact the immediate autophagic response to starvation is triggered by amino acid deficiency independently of mTOR and substrates of the immediate autophagic response to starvation are associated with the endosomal network (Mejlvang et al. 2018). However, particularly during starvation, the endosomal network rapidly acidifies and the rapid degradation triggered by amino acid starvation is dependent mainly on the lysosome (Lefebvre et al. 2018). These findings, coupled to the chemical characteristics of the molecule, seem to highlight that AJ2NBD labels endosomes and only first steps of endosome maturation, until they reach a clear acid pH. In fact, at pH around 4.5, the contribution of deprotonated $H_2AJ2NBD^{2+}$ species is relevant and, due to the great positive charge, its ability to enter the membrane of the vacuoles/vesicles is significatively lower than at pH > 6, when the less charged form $HAJ2NBD^{+}$ is prevalent (Figure 1). These results were further confirmed by the study of colocalization between AJ2NBD and LDTR in response to two different triggers, showing a different fluorescence distribution and Pearson coefficients between starved and rapamycin-treated cells (Figure 5 C and D).

Discussion

In the last decade, a great research work on different probes able to trace the localization and the functions of the organelles have been performed (Zhu et al. 2016). Here we present a new probe, AJ2NBD, able to display excellent fluorescent properties coupled with absence of cytotoxicity, that make it a suitable tool for living cell studying.

This newly synthesized molecule contains two NBD fluorophore units linked to a tetraaza macrocycle and merges interesting photochemical properties with a peculiar acid-base behavior. In fact, in the pH-range 2–11 three species of the probe can exist, namely $H_2AJ2NBD^{2+}$in the 2.0–4.2 pH-range, $HAJ2NBD^{2+}$(4.2–9.7), AJ2NBD (9.7–11). The ligand shows an evident solvato-chromism being its emission quantum yield strongly influenced by the physical-chemical characteristics of the environment such

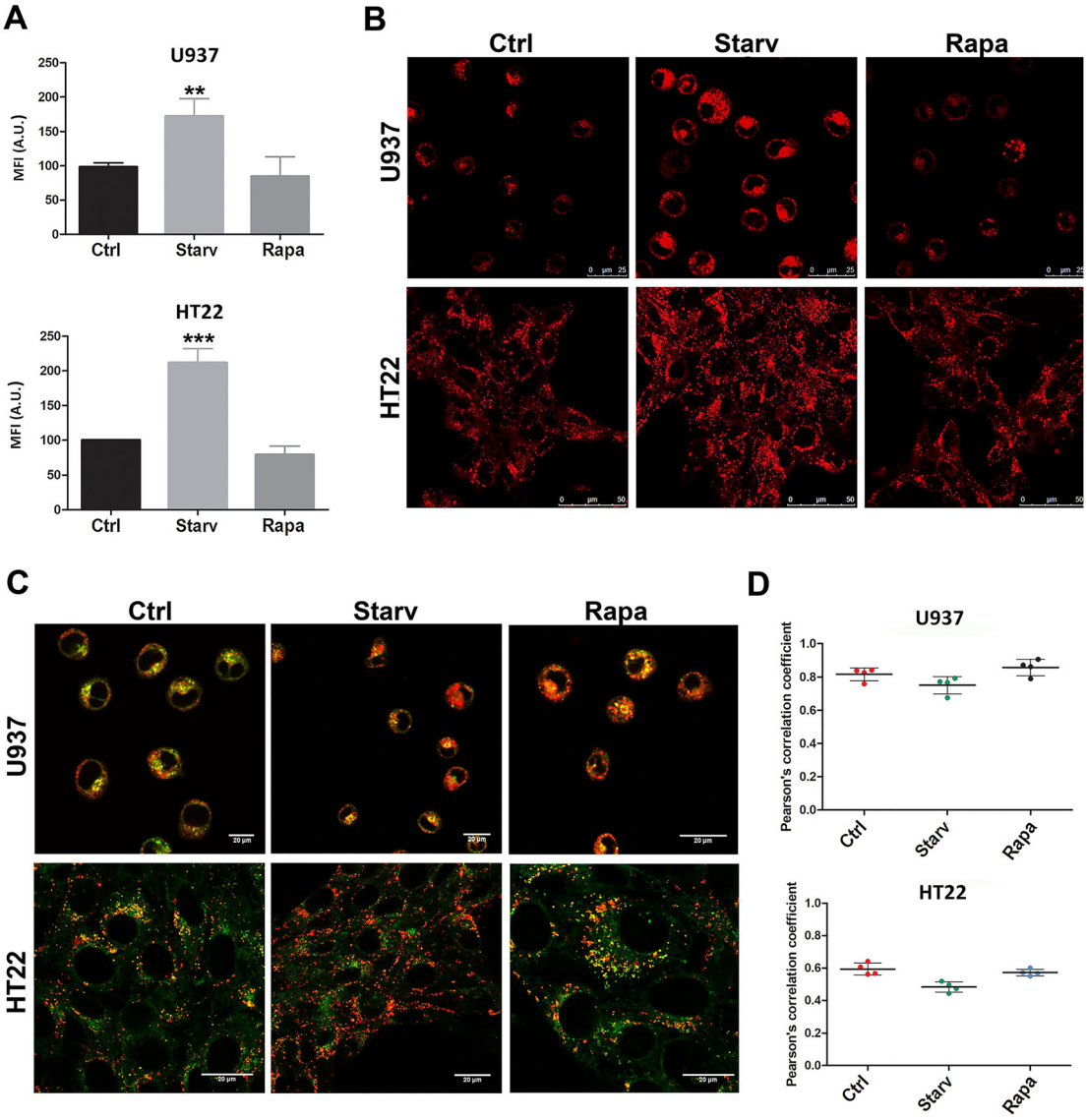

Figure 5: Detection of acid-lysosomal compartment by AJ2NBD and LTDR co-labelling in starved and rapamycin-treated cells.
(A) Statistical histogram of LTDR MFI on U937 and HT22 control (ctrl), starved (Starv) and rapamycin treated cells (Rapa). (B) Confocal images of LTDR staining in U937 and HT22 control (ctrl), starved (Starv) and rapamycin-treated cells (Rapa). Scale bars: 25 and 50 µm. (C) Colocalization between AJ2NBD and LTDR staining in U937 and HT22 control (ctrl), starved (Starv) and rapamycin-treated cells (Rapa). The confocal images of HT22 and U937 show a greater colocalization in ctrl and Rapa if compared to Starv condition. Scale bars: 20 µm. (D) the colocalization in HT22 and U937 cell lines has been quantified by Pearson coefficient. Each value is expressed as the mean ± SD (results from $n \geq 3$ independent experiments); one-way ANOVA with Bonferroni's multiple comparison test revealed: $^{**}p < 0.01$, and $^{***}p < 0.001$ vs. control.

as polarity, dielectric constant or H-bond donor capability of the solvent, moreover in aqueous solution the emission intensity depends on the pH. Thus, due to these characteristics and considering that also the capability of penetrating biological membranes is influenced by pH, the overall photochemical behavior of the ligand can be profoundly different in the various cellular compartments.

From a biologic point of view, the AJ2NBD probe shows a stable fluorescent signal, a resistance to photobleaching and a specific labelling in a lower range of concentrations (i.e. 200 and 500 nM). Furthermore, the AJ2NBD protocol staining is relatively simple and suitable for living cells so our results lead us to identify it as vital dye. In addition, the stain with AJ2NBD did not interfere with other commercial dyes (i.e. MTR, LDTR) demonstrating its suitability in the biological studies characterized by the concurrent application of different probes, as we have performed in the results section. On the other hand, the staining performed

on AJ2NBD fixed cells does not allow us to report specific results. When the labelling is performed on living HT22 and U937 cell lines, our probe, AJ2NBD stains a perinuclear area in the specific region around the Golgi in which it seems to mark the numerous newly formed vesicles in the Juxta-Golgi region (Figure 3). The trans-Golgi network is identified as the site where the recycling endosomes budded. Our findings showed that AJ2NBD specifically stained a specific region around the Golgi also co-labeled with LTDR demonstrating a partial colocalization between AJ2NBD and LTDR in both cell lines investigated. Accordingly, to evaluate the possibility to apply AJ2NBD in studying where the vesicular formation and trafficking play a key role, we treated the cells with the specific autophagic triggers such as serum deprivation and rapamycin.

Autophagy is defined as an important pathway for maintaining cell homeostasis. Autophagy has been traditionally linked to cellular energy balance and to the cellular nutritional status (Singh and Cuervo 2011, 2012). Endocytosis shows several parallels with autophagy, in fact the endosome system functions in importing nutrients and macromolecules into the cell from outside (Hyttinen et al. 2013).

Our findings demonstrated that AJ2NBD is able to follow neutral vesicle quantification and trafficking in response to the two different triggers. In detail, we found that AJ2NBD mainly labels endosomes and the first steps of endosome maturation, until they reach a clear acid pH. Due to their different capacities of acidification, a stable pH gradient is established in different compartments during the maturation process: early endosomes maintain pH at about 6.5, late endosomes at about 5.5 and lysosomes at about 4.5 (Hu et al. 2015).

Indeed, the chemical characteristics of the AJ2NBD molecule, and in particular its acid-base behavior, allow it to enter the membrane of the early endosomes, but when the tri-protonated form prevails (at pH: 4, 5.5) the capability of the probe to enter the membrane of more acid vacuoles drastically decreases and therefore not displaying its characteristic fluorescence.

Nowadays several technical approaches have been described to investigate the autophagy and endocytosis, respectively. However, recent evidence has displayed an interplay between these two pathways, so the identification of new probes might represent an important tool for this research's field. The process of how autophagosomes and endosomes are driven to fuse with lysosomes is one of the crucial steps in autophagy and endocytosis. For this reason, the identification of new probes is increasingly topical in this research's field. We propose the following cartoon (Figure 6) to illustrate the intracellular compartments labelled by AJ2NBD, however, to ensure the precise nature of vesicles/vacuoles traced by this new probe, other more specific tests are in progress.

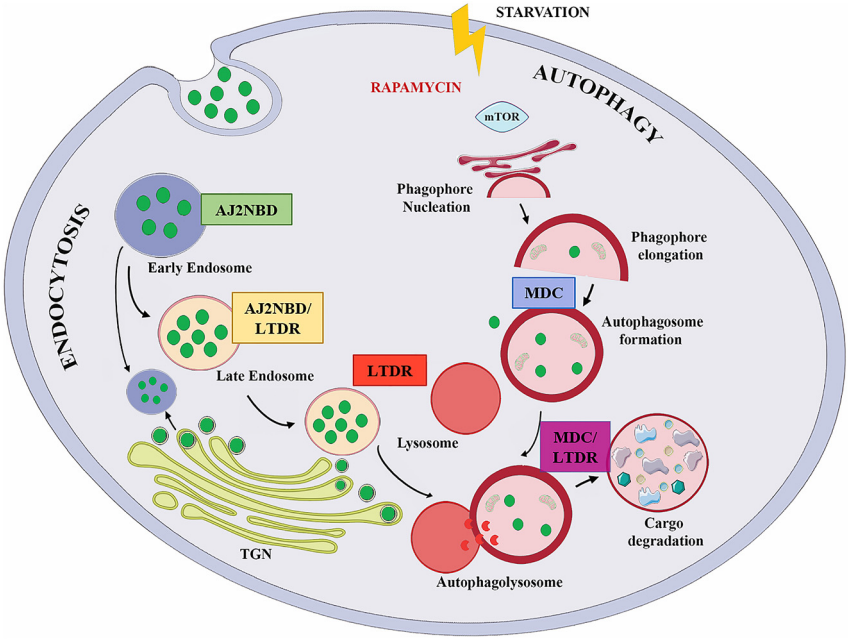

Figure 6: Graphical representation of intracellular compartments labelled, co-labelled, unlabeled by AJ2NBD.

Materials and methods

Synthesis

Probe AJ2NBD was obtained following the synthetic procedure reported in Scheme 1. 1,7-dimethyl-1,4,7,10-tetraazacyclododecane (1) was prepared as previously described (Ciampolini et al. 1984).

1,7-bis (7-nitrobenzo[1,2,5]oxadiazole-4-yl)-4,10-dimethyl-1,4,7,10-tetraazacyclododecane tetrahydrochloride (AJ2NBD·4HCl)

1,7-dimethyl-1,4,7,10-tetraazacyclododecane (1) (1 g, 5 mmol) and K_2CO_3 (10.2 g, 74 mmol) were suspended in acetonitrile (100 cm^3). 4-chloro-7-nitrobenzo-1,2,5-oxadiazole (2) (2.2 g, 11 mmol) in acetonitrile (80 cm^3) was added drop-wise over 1 h, after which the suspension was stirred at room temperature for 48 h and then filtered. The solution was evaporated under vacuum to yield the crude product, and the orange solid obtained was recrystallized from hot ethanol/37% aqueous HCl obtaining L·4HCl (2.7 g, 80%). $C_{22}H_{30}Cl_4N_{10}O_6$: C, 39.30; H, 4.50; N, 20.83. Found: C, 39.5; H, 4.7; N, 20.6. ^{1}H NMR (DMSO-d_6, 30 °C, δ in ppm): 2.92 (*s*, 6H), 3.14 (*m*, 4H), 3.35 (*m*, 4H), 4.41 (*m*, 8H), 6.42 (*d*, *J* = 9.2 Hz, 2H), 8.52 (*d*, *J* = 9.2 Hz, 2H), 13.46 (br s, 1H). ^{13}C NMR (DMSO-d_6, 30 °C, δ in ppm): 41.0, 51.7, 58.7, 103.7, 121.8, 136.5, 145.1, 145.5, 145.9.

Elemental analyses

Elemental analyses were performed with a Thermo Finnigan Flash 1112 EA CHN analyzer.

NMR spectra

^{1}H- and ^{13}C-NMR spectra were recorded on a Bruker Avance 400 instrument, operating at 400.13 and 100.61 MHz, respectively, and equipped with a variable temperature controller. The temperature of the NMR probe was calibrated using 1,2-ethanediol as calibration sample. For the spectra recorded in DMSO-d_6 the ^{1}H and ^{13}C peak positions are reported with respect to the residual solvent peak. Chemical shifts (δ scale) are reported in parts per million (ppm values) and coupling constants (*J* values) are given in hertz (Hz).

UV–Vis and fluorescence spectra

UV–Vis absorption spectra were recorded at 298.1 K on a Varian Cary-100 spectrophotometer equipped with a temperature control unit. Fluorescence emission spectra were recorded at 298.1 K on a Varian Cary-Eclipse spectrofluorimeter and the spectra are uncorrected. The fluorescence quantum yields of fully protonated ligands (φ_{fl}) were determined by comparing the integrated fluorescence spectra of the sample with fluorescein in 0.1 mol dm^{-3} NaOH (φ_{fl} = 0.925) (Magde et al. 2002).

Spectrophotometric titrations

In a typical experiment, a 0.1 mol dm^{-3} NaOH solution was added in small amounts to the solution containing the ligand and the pH was measured after at least 10 min. At least three sets of spectrophotometric pH titration curves were performed. All sets of curves were treated either as single sets or as separate entities, for each system; no significant variations were found in the values of the determined constants. The HypSpec computer program was used to process the spectrophotometric data (Gans et al. 1996).

Cell culture and treatment

U937 cells were cultured in 25 cm^2 flasks in RPMI 1640, supplemented with 10% fetal bovine serum (FBS), L-glutamine (100 mM) and 1% antibiotics (penicillin, streptomycin). Hippocampal HT22 cells were maintained in DMEM-HAM'S F12, supplemented with 10% FBS, L-glutamine (100 mM) and 1% antibiotics (penicillin, streptomycin). The two cell lines were incubated in a humidified 5% CO_2 atmosphere at 37 °C. At 80% confluence HT22 cells were detached with trypsin-EDTA, washed and sub-cultivated in new flasks for 1–2 days before the experiments.

For the serum starvation experiments HT22 cells were washed in PBS and maintained in culture medium without FBS at 37 °C and 5% CO_2 in humidified air overnight (24 h) until analysis (Cesarini et al. 2018). For the U937 cells the serum starvation was performed for 4 h in the same experimental conditions. For rapamycin-induced autophagy, the rapamycin was used at 100 nM for 4 h in U937 and at 250 nM for 18 h in HT22 cells, respectively (Galati et al. 2019)

Trypan Blue test

U937 cells were stained with different commercial probes and AJ2NBD probes in order to evaluated the cytotoxicity of the new probe. The cells were collected and centrifuged at 1200 rpm for 5 min. Cells were then resuspended in an equivalent volume of 0.4% Trypan Blue solution and counted with a Burker's chamber under light microscopy. Cells excluding Trypan blue were considered viable.

Confocal microscopy

AJ2NBD was dissolved in DMSO at the final concentration of 15 mM. Cells were incubated at 37 °C with 500 nM (f.c.) of AJ2NBD for 30 min. At the end of the incubation time, cells were washed with PBS and stained with other fluorophores in order to understand the specificity of dye. Mitochondrial mass, lysosomal content and Golgi complex were also detected by confocal microscopy. To evaluate the mitochondrial morphology the cells were grown on MatTek glass bottom chambers (MatTek Corporation) and stained with MitoTracker Red (MTR) 200 nM (f.c.) for 20 min at 37 °C in 5% CO_2. To evaluate the lysosomal and acidic vesicular organelle formation the cells were stained $_{with}$ LysoTracker Deep Red (LTDR) 100 nM and the pH-sensitive dye Acridine Orange (AO; Sigma-Aldrich, St. Louis, MO, USA) 75 ng/ml for 30 min at 37 °C in 5% CO_2, respectively. The Golgi complex was visualized by BODIPY™ TR Ceramide complexed to BSA (B34400 Invitrogen™). Briefly, the cells were washed in HBSS and incubated at 4 °C with 5 μM BodipyTR Ceramide in the same medium. The cells were

washed three times and then incubated for a further 30 min. The images were acquired by a Leica TCS SP5 II confocal microscope (Leica Microsystem, Germany) with 488, 543 and 633 nm illumination and oil-immersed objectives, and averaged in real time using a line average to reduce random noise (Canonico et al. 2016). The images were further processed and analyzed in ImageJ software (National Institutes of Health, Bethesda, MD, USA). Colocalization analyses (Pearson's correlation coefficient) were performed using JACoP plugin in ImageJ (Bolte and Cordelières 2006). Pearson's coefficients were derived from three completely independent experiments with >3 fields contributing to the cumulative result.

Flow cytometric staining

The probes investigated by confocal microscopy were also employed in flow cytometry with the same protocols. In detail, the concentration of MTR and LTDR employed was lower (50 nM) if compared to the microscopical analyses, while in the same way the concentration of AJ2NBD was 200 nM. Furthermore, we also measured the acid compartment by flow cytometry using 75 ng/ml (f.c.) of AO. AO is a cell-permeable fluorescent dye that, at its highest concentrations, stains the double stranded DNA red green and the cytoplasm bright green red. It can also enter acidic compartments, such as lysosomes and autolysosomes, where it becomes protonated and sequestered. In these compartments, at its lowest concentrations, in an acid environment, AO emits red fluorescence with an intensity proportional to the degree of acidity and/or to the acidic compartment volume (Canonico et al. 2018; Traganos and Darzynkiewicz 1994). Red lysosomal and green cytoplasmic fluorescence were acquired by flow cytometry using the FL3 and FL1 channels, respectively. In order to assess the compatibility of AJ2NBD for the biological studies, the cells were also stained with Bodipy 1 μg/ml for 30 min at 37 °C in 5% CO_2. Following induction of autophagy, the cells were incubated with 50 μM MDC in order to evaluate the autophagic vacuoles. After the staining, the adherent cells were harvested by trypsinization, washed and then resuspended in PBS for the cytometric analysis. Cytometric experiments were carried out with a FACSCanto II flow cytometer (BD Biosciences) equipped with blue (488 nm, air-cooled, 20 mW solid state), red (633 nm, 17 mW HeNe), and violet (405 nm, 30 mW solid state) lasers. Analyses were performed with FACSDivaTM software (BD Biosciences). Samples were acquired by flow cytometry, collecting at least 10,000 events from each tube.

Statistical analyses

Quantitative data are expressed as mean ± SD on the basis of at least three independent experiments. Differences between groups were analyzed using a One-way analysis of variance (one-way ANOVA), followed by Bonferroni post hoc Test. A p-value <0.05 was considered significant. All statistical analyses were performed using GraphPad Prism 5.0 (GraphPad software).

Author contributions: All the authors have accepted responsibility for the entire content of this submitted manuscript and approved submission.
Research funding: None declared.
Conflict of interest statement: The authors declare no conflicts of interest regarding this article.

References

Amatori, S., Ambrosi, G., Borgogelli, E., Fanelli, M., Formica, M., Fusi, V., Giorgi, L., Macedi, E., Micheloni, M., Paoli, P., et al. (2014). Modulating the sensor response to halide using NBD-based azamacrocycles. Inorg. Chem. 53: 4560–4569.

Amatori, S., Ambrosi, G., Fanelli, M., Formica, M., Fusi, V., Giorgi, L., Macedi, E., Micheloni, M., Paoli, P., Pontellini, R., et al. (2012). Multi-use NBD-based tetra-amino macrocycle: fluorescent probe for metals and anions and live cell marker. Chemistry 18: 4274–4284.

Ambrosi, G., Ciattini, S., Formica, M., Fusi, V., Giorgi, L., Macedi, E., Micheloni, M., Paoli, P., Rossi, P., and Zappia, G. (2009). A new versatile solvatochromic amino-macrocycle. from metal ions to cell sensing in solution and in the solid state. Chem. Commun. 45: 7039–7041.

Arca, M., Caltagirone, C., De Filippo, G., Formica, M., Fusi, V., Giorgi, L., Lippolis, V., Prodi, L., Rampazzo, E., Scorciapino, M.A., et al. (2014). A fluorescent ratiometric nanosized system for the determination of PdII in water. Chem. Commun. 50: 15259–15262.

Bolte, S. and Cordelières, F.P. (2006). A guided tour into subcellular colocalization analysis in light microscopy. J. Microsc. 224: 213–232.

Canonico, B., Cesarini, E., Salucci, S., Luchetti, F., Falcieri, E., Di Sario, G., Palma, F., and Papa, S. (2016). Defective autophagy, mitochondrial clearance and lipophagy in niemann-pick type B lymphocytes. PLoS One, https://doi.org/10.1371/journal.pone.0165780.

Canonico, B., Di Sario, G., Cesarini, E., Campana, R., Luchetti, F., Zamai, L., Ortolani, C., Nasoni, M.G., Baffone, W., and Papa, S. (2018). Monocyte response to different Campylobacter jejuni lysates involves endoplasmic reticulum stress and the lysosomal–mitochondrial axis: when cell death is better than cell survival. Toxins 10, https://doi.org/10.3390/toxins10060239.

Cao, Z., Wang, Y., Long, Z., and He, G. (2019). Interaction between autophagy and the NLRP3 inflammasome. Acta Biochim. Biophys. Sin. https://doi.org/10.1093/abbs/gmz098.

Cesarini, E., Cerioni, L., Canonico, B., Di Sario, G., Guidarelli, A., Lattanzi, D., Savelli, D., Guescini, M., Nasoni, M.G., Bigini, N., et al. (2018). Melatonin protects hippocampal HT22 cells from the effects of serum deprivation specifically targeting mitochondria. PloS One 13: e0203001.

Ciampolini, M., Micheloni, M., Nardi, N., Paoletti, P., Dapporto, P., and Zanobini, F. (1984). Synthesis and characterisation of 1,7-dimethyl-1,4,7,10-tetra-azacyclododecane: crystal structure of the nickel(II) bromide monohydrate complex of this macrocycle; thermodynamic studies of protonation and metal complex formation. Dalton Trans. 7: 1357–1362.

Dick, F.P., Coelho, F.L., Rodembusch, F.S., and Campo, L.F. (2014). Amphiphilic ESIPT benzoxazole derivatives as prospective fluorescent membrane probes. Tetrahedron Lett. 55: 3024–3029.

Formica, M., Fusi, V., Giorgi, L., and Micheloni, M. (2012). New fluorescent chemosensors for metal ions in solution. Coord. Chem. Rev. https://doi.org/10.1016/j.ccr.2011.09.010.

Galati, S., Boni, C., Gerra, M.C., Lazzaretti, M., and Buschini, A. (2019). Autophagy: a player in response to oxidative stress and DNA damage. Oxidative Medicine and Cellular Longevity, https://doi.org/10.1155/2019/5692958.

Gans, P., Sabatini, A., and Vacca, A. (1996). Investigation of equilibria in solution. Determination of equilibrium constants with the HYPERQUAD suite of programs. Talanta 43: 1739–1753.

Hu, Y.B., Dammer, E.B., Ren, R.J., and Wang, G. (2015). The endosomal-lysosomal system: from acidification and cargo sorting to neurodegeneration. Transl. Neurodegener. 4: 1–10.

Hyttinen, J.M.T., Niittykoski, M., Salminen, A., and Kaarniranta, K. (2013). Maturation of autophagosomes and endosomes: a key role for Rab7. Biochim. Biophys. Acta Mol. Cell Res. 1833: 503–510.

Klionsky, D.J., Abdel-Aziz, A.K., Abdelfatah, S., Abdellatif, M., Abdoli, A., Abel, S., Abeliovich, H., Abildgaard, M.H., Abudu, Y.P., and Acevedo-Arozena, A., et al. (2021). Guidelines for the use and interpretation of assays for monitoring autophagy (4th edition). Autophagy 17: 1–382.

Lefebvre, C., Legouis, R., and Culetto, E. (2018). ESCRT and autophagies: endosomal functions and beyond. Semin. Cell Dev. Biol. 74: 21–28.

Magde, D., Wong, R., and Seybold, P.G. (2002). Fluorescence quantum yields and their relation to lifetimes of Rhodamine 6G and fluorescein in nine solvents: improved absolute standards for quantum yields. Photochem. Photobiol. 75: 327–334.

Marshansky, V. and Futai, M. (2008). The V-type H^+-ATPase in vesicular trafficking: targeting, regulation and function. Curr. Opin. Cell Biol. 20: 415–426.

Mejlvang, J., Olsvik, H., Svenning, S., Bruun, J.A., Abudu, Y.P., Larsen, K.B., Brech, A., Hansen, T.E., Brenne, H., Hansen, T., et al. (2018). Starvation induces rapid degradation of selective autophagy receptors by endosomal microautophagy. JCB (J. Cell Biol.) 217: 3640–3655.

Papa, S., Luchetti, F., Canonico, B., Fusi, V., Formica, M., and Giorgi, L. (2019). *Preparation of heterocyclic compounds as fluorescent probes for detection in biological systems*. Patent Information: Apr 25, 2019 - WO 2019077527 A1, Application: Oct 17, 2018 - WO 2018-IB58063. Priority: Oct 17, 2017 - IT 2017-117226.

Ravikumar, B., Moreau, K., Jahreiss, L., Puri, C., and Rubinsztein, D.C. (2010). Plasma membrane contributes to the formation of pre-autophagosomal structures. Nat. Cell Biol. 12: 747–757.

Razi, M., Chan, E.Y.W., and Tooze, S.A. (2009). Early endosomes and endosomal coatomer are required for autophagy. JCB (J. Cell Biol.) 185: 305–321.

Schreij, A.M.A., Fon, E.A., and McPherson, P.S. (2016). Endocytic membrane trafficking and neurodegenerative disease. Cell. Mol. Life Sci. https://doi.org/10.1007/s00018-015-2105-x.

Singh, R. and Cuervo, A.M. (2011). Autophagy in the cellular energetic balance. Cell Metabol. 13: 495–504.

Singh, R. and Cuervo, A.M. (2012). Lipophagy: connecting autophagy and lipid metabolism. Int. J. Cell Biol., https://doi.org/10.1155/2012/282041.

Traganos, F. and Darzynkiewicz, Z. (1994). Lysosomal proton pump activity: supravital cell staining with acridine orange differentiates leukocyte subpopulations. Methods Cell Biol. https://doi.org/10.1016/S0091-679X(08)61717-3.

Uchiyama, S., Santa, T., Fukushima, T., Homma, H., and Imai, K. (1998). Effects of the substituent groups at the 4- and 7-positions on the fluorescence characteristics of benzofurazan compounds. Perkin Trans. 2: 2165–2173.

Uchiyama, S., Santa, T., and Imai, K. (1999). Semi-empirical PM3 calculation reveals the relationship between the fluorescence characteristics of 4,7-disubstituted benzofurazan compounds, the LUMO energy and the dipole moment directed from the 4- to the 7-position. Perkin Trans. 3: 569–576.

Wang, L., Wan, J., Zhao, Y., Yang, N., and Wang, D. (2019). Hollow multi-shelled structures of Co3O4 dodecahedron with unique crystal orientation for enhanced photocatalytic CO2 reduction. J. Am. Chem. Soc. 141: 2238–2241.

Xu, W., Zeng, Z., Jiang, J.H., Chang, Y.T., and Yuan, L. (2016). Discerning the chemistry in individual organelles with small-molecule fluorescent probes. Angew. Chem. Int. Ed. 55: 13658–13699.

Zhu, H., Fan, J., Du, J., and Peng, X. (2016). Fluorescent probes for sensing and imaging within specific cellular organelles. Acc. Chem. Res. 49: 2115–2126.

Supplementary Material: The online version of this article offers supplementary material (https://doi.org/10.1515/hsz-2021-0204).